Available online at www.sciencedirect.com
SCIENCE DIRECT®
Journal of Solid State Chemistry 177 (2004) 3140–3148
JOURNAL OF SOLID STATE CHEMISTRY
http://elsevier.com/locate/jssc

Cubic perovskite-related phases in the ternary SrO–CuO–Nb_2O_5 system

Yun Liu, Ray L. Withers,* Frank Brink,[1] and Lasse Norén

Research School of Chemistry, Australian National University, GPO Box 4, Science Road, Canberra ACT 0200, Australia

Received 9 November 2003; received in revised form 11 May 2004; accepted 12 May 2004

Available online 15 July 2004

Abstract

A careful phase analysis study of cubic perovskite-related phases in the ternary SrO–CuO–Nb_2O_5 system has been carried out via the synthesis and compositional analysis of a range of specimens within the ternary SrO–CuO–Nb_2O_5 system. Powder XRD in conjunction with electron probe microanalysis (EPMA) has been used to determine whether the synthesized specimens are single phase or not and to determine the compositions of the various reaction products. Three quite distinct such solid solution phases have been found and their quite distinct electrical and diffraction characteristics investigated.

Keywords: SrO–CuO–Nb_2O_5 system; Perovskite-related phases therein

1. Introduction

Ever since the discovery of high-temperature superconductivity [1] in materials such as the cubic perovskite-related $YBa_2Cu_3O_{7-\delta}$ system (and the subsequent realization of the crucial role played by Cu ions in the superconducting state), Cu-containing materials and their physico-chemical properties have been the subject of renewed and often intensive investigation [2–6]. Well before the discovery of high-temperature superconductivity, however, Cu-containing, cubic perovskite-related materials had already been reported to possess intriguing and potentially useful physical properties. Venevtsev [7], for example, as far back as 1971 reported that all eleven copper containing complex perovskite phases then known, including each of the A_2CuWO_6 (A = Sr or Ba; $\equiv ACu_{1/2}W_{1/2}O_3$) and $A_3CuB_2O_9$ (A = Sr or Ba; B = Nb or Ta; $\equiv ACu_{1/3}B_{2/3}O_3$) phases, were ferroelectrics with high Curie temperatures and that it was therefore "…especially important to synthesize and to investigate Cu-containing perovskites…". Despite the recent general surge of interest in Cu-containing, perovskite-related phases, there has to date still been relatively little detailed investigation of any of the members of this family of phases.

Very recently, Sun et al. [8] reported the simple cubic structure and magnetic properties of a cubic perovskite type, $Sr_2CuNbO_{5.25}$ ($\equiv SrCu_{1/2}Nb_{1/2}O_{2.625}$) compound synthesized from monoxide and carbonate starting materials. Tao and Irvine [9], on the other hand, in a structure and conductivity study of the $Sr_3Cu_{1+y}Nb_{2-y}O_{9-\delta}$, $0 \leqslant y \leqslant 1$ ($\equiv SrCu_{1/3\cdot(1+y)}Nb_{1/3\cdot(2-y)}O_{1/3\cdot(9-\delta)}$) system were unable to obtain single phase material either at the $y = 0.5$ composition, equivalent to the composition reported by Sun et al. [8], or at the $y = 0$ composition, corresponding to the $Sr_3CuNb_2O_9$ ($\equiv SrCu_{1/3}Nb_{2/3}O_3$) composition originally reported by Venevtsev [7]. Instead these authors reported that phase purity could only be obtained for $y = 0.2$, at which stage a tetragonal (but very close to metrically cubic) $Sr_3Cu_{1.2}Nb_{1.8}O_{8.7}$ ($\equiv SrCu_{0.4}Nb_{0.6}O_{2.9}$) perovskite-related phase was found. In 1992, Fesenko et al. [10] also reported difficulties in reproducing single phase $Sr_3CuNb_2O_9$ ($\equiv SrCu_{1/3}Nb_{2/3}O_3$) material from monoxide and carbonate starting materials, although single phase material at this composition was reported provided appropriate

*Corresponding author. Fax: +61-2-6125-0750.
E-mail address: withers@rsc.anu.edu.au (R.L. Withers).
[1] Also at the Electron Microscope Unit, Research School of Biological Sciences, Australian National University, Canberra ACT 0200, Australia.

0022-4596/$ - see front matter © 2004 Elsevier Inc. All rights reserved.
doi:10.1016/j.jssc.2004.05.028

intermediate binary oxides were used and the temperature was not too high.

Finally, Podkorytov et al. [11], in a careful study of the mechanism of formation of $(Sr_{1-y}Cu_y)_2Nb_2O_7$ and $(Sr_{1-y}Cu_y)_4Nb_2O_9$ solid solution phases in the same ternary $SrCO_3$–Nb_2O_5–CuO system, showed that the primary intermediate synthesis product below $\sim$1000°C was always a composition within the $(Sr_{1-y}Cu_y)_5Nb_4O_{15}$ solid solution phase which subsequently underwent further solid phase reactions with other intermediate products or SrO above 1000°C. They demonstrated the complexity of the various solid phase reactions involved in the ternary $SrCO_3$–Nb_2O_5–CuO system and the importance of both kinetic as well as thermodynamic and structural factors in determining the final reaction products. These authors reported a continuous $(Sr_{1-y}Cu_y)_4Nb_2O_9$, $0 \leqslant y \leqslant 0.25$, perovskite-related solid solution all the way from $Sr_4Nb_2O_9$ ($\equiv SrSr_{1/3}Nb_{2/3}O_3$) to $Sr_3Cu_1Nb_2O_9$ ($\equiv SrCu_{1/3}Nb_{2/3}O_3$).

Given the absence of any detailed microanalytical or structural investigation of these materials as well as the contradictory nature of much of the reported information described above as regards the number and composition range of distinct cubic perovskite-related solid solution phases within the ternary SrO–CuO–Nb_2O_5 system, it was therefore decided to carefully re-investigate this ternary system from the phase analysis point of view, focussing on cubic perovskite-related phases therein.

As seen above there are various ways to write the stoichiometry of complex perovskite compounds. In order to maintain a consistent notation, we will from here on write the composition of these perovskite-related solid solution phases in the form $Sr_{\sim 1}Cu_xNb_{1-x}O_{3-\delta}$.

2. Experimental

Compounds in the SrO–CuO–Nb_2O_5 system were synthesized by solid-state reaction using strontium carbonate ($SrCO_3$, 5 N, Alfa), copper (II) oxide (CuO, 4 N, Aldrich) and niobium (V) pentoxide (Nb_2O_5, >3 N, Alfa) as starting materials. Powders of the desired stoichiometry were thoroughly mixed in a mortar and then thermally treated at 850°C for an initial period of 20 h. The resultant powders were then mixed, pressed into a pellet and sintered in the range of 1050–1500°C for successive periods until there were no further changes observed in the XRD patterns.

The resultant samples were then carefully investigated by powder X-ray diffraction using a Guinier–Hägg camera with a Cu$K\alpha_1$ radiation source. Si (NBS ♯640c, $a = 5.431195(9)$ Å at 22.5°C) was used as an internal standard in order to accurately determine unit cell parameters through the "Unitcell" software package [12].

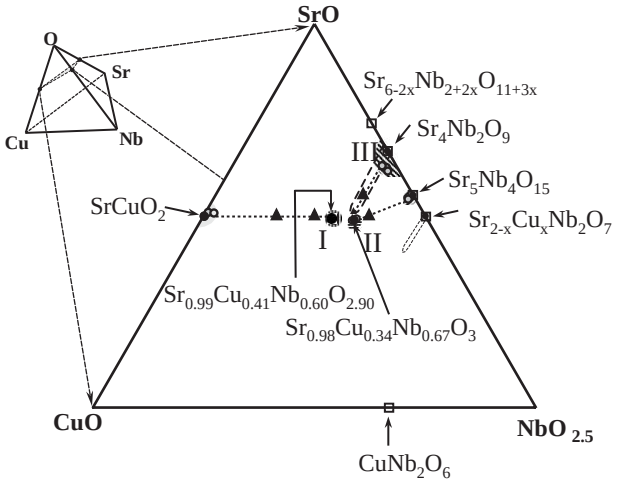

Fig. 1. Specimens synthesized within the SrO–CuO–$NbO_{2.5}$ ternary system. Single phase samples are represented by round circles, ideal compositions by the filled circles and two phase samples by the empty triangles. The empty squares come from Ref. [11]. The three distinct cubic perovskite-related solution regions are labelled by I, II and III, respectively.

Composition was carefully determined by Electron Probe Microanalysis (EPMA) at 15 kV and 2 nA using a JEOL 6400 Scanning Electron Microscope (SEM) equipped with an Oxford Instruments light element EDS detector and Link ISIS SEMquant software. Pure Cu and synthesized single phase $Sr_5Nb_4O_{15}$ were used as calibration standards, the latter in order to minimize the atomic number, absorption and fluoresence (ZAF) corrections for EPMA analysis of other specimens within the SrO–CuO–Nb_2O_5 system (see Fig. 1). EPMA analysis of synthesized single phase $Sr_2Nb_2O_7$ gave a composition of $Sr_{1.99(1)}Nb_{2.00(1)}O_7$ confirming the appropriateness of $Sr_5Nb_4O_{15}$ as a calibration standard.

EDPs were obtained using a Philips EM 430 transmission electron microscope operating at 300 kV on crushed grains of the samples dispersed on holey carbon coated copper grids. The electrical conductivity of pelletized samples was measured in air up to 770 K using a HP 3478 A multimeter in four wires mode. The maximum resistance measurable via this apparatus was 30 MΩ.

3. Results and discussion

3.1. Phase analysis and EPMA results

In agreement with Tao and Irvine [9], we found that the synthesized $SrCu_xNb_{1-x}O_{3-\delta}$, $x = 0.5$, sample was always consistently two phase, with the majority phase

corresponding to the end member of a metrically cubic, perovskite-related solid solution phase and the minority phase to an $SrCuO_2$-related solid solution phase (see Fig. 1). Grains of both phases were quite readily found in the SEM and carefully analyzed by EPMA. The average of 10 separate analyses of the perovskite-related solid solution phase gave a composition of $Sr_{0.98(3)}Cu_{0.42(2)}Nb_{0.59(2)}O_{2.88}$, very close to the $x = 0.2$, $SrCu_{0.4}Nb_{0.6}O_{2.9}$, composition reported by Tao and Irvine [9]. The average of 10 separate analyses of the $SrCuO_2$-related phase gave a composition of $Sr_{1.00(2)}Cu_{0.98(2)}Nb_{0.01(1)}O_2$. Note that we have assumed all the Cu is in the 2+ oxidation state and used charge balance to determine the oxygen content while the errors quoted simply reflect the reproducibility of the separate analyses. As an independent check of the existence of this cubic perovskite-related solid solution, a single phase (to XRD) specimen of nominal composition $SrCu_{0.42}Nb_{0.58}O_{2.87}$ was also synthesized. EPMA analysis of this phase gave a composition of $Sr_{0.99(2)}Cu_{0.41(1)}Nb_{0.60(1)}O_{2.90}$. We label this narrow, cubic perovskite-related solid solution phase SS-I.

In agreement with the results of Venevtsev et al. [7], an essentially single phase (although see Section 3.2 below), very close to metrically tetragonal specimen of nominal composition $SrCu_{0.33}Nb_{0.67}O_3$ was also able to be be consistently synthesized provided the synthesis conditions (in particular, the final annealing temperature of 1300°C) were carefully controlled. Given that a trace amount of an $Sr_5Nb_4O_{15}$ related phase was detected in XRD patterns from this sample (in agreement with Tao and Irvine [9], see Section 3.2 below), its composition was carefully analyzed within individual grains by EPMA. The average of 10 separate analyses gave $Sr_{0.98(2)}Cu_{0.34(2)}Nb_{0.67(1)}O_3$ as the overall composition, again in very good agreement with the nominal $SrCu_{0.33}Nb_{0.67}O_3$ stoichiometry. We label this compositionally close but quite distinct cubic perovskite-related solid solution phase based on the ideal $SrCu_{0.33}Nb_{0.67}O_3$ stoichiometry SS-II (see the tentative phase diagram given in Fig. 1).

To further investigate the composition range of this cubic perovskite-related solid solution phase, an additional sample of nominal composition $SrCu_{0.25}Nb_{0.75}O_{3.125}$ (see Fig. 1) was also synthesized. The sample was clearly two phase, with the majority phase corresponding to the end member of the SS-II solid solution and the other phase to an $Sr_5Nb_4O_{15}$ related phase. Grains of both phases were quite readily found in the SEM and carefully analyzed by EPMA. The average of 10 separate analyses of the perovskite-related solid solution phase gave a composition of $Sr_{0.98(1)}Cu_{0.32(1)}Nb_{0.68(1)}O_3$, very close to the nominal $SrCu_{0.33}Nb_{0.67}O_3$ composition for this phase. The average of 10 separate analyses of the $Sr_5Nb_4O_{15}$-related phase gave a composition of $Sr_{4.90(8)}Cu_{0.13(7)}Nb_{3.99(9)}O_{15}$. Clearly the SS-II phase only exists for a Nb/Cu ratio very close to 2:1.

A third cubic perovskite-related solid solution phase (labelled SS-III in Fig. 1), based on the composition $Sr_4Nb_2O_9$ ($\equiv Sr(Sr_{1/3}Nb_{2/3})O_3$) but capable of considerable substitution of Cu for Sr, was also found to exist. Podkorytov et al. [11], in fact, reported a continuous $(Sr_{1-y}Cu_y)_4Nb_2O_9$, $0 \leqslant y \leqslant 0.25$, perovskite-related solid solution all the way from metrically cubic $Sr_4Nb_2O_9$ ($\equiv Sr(Sr_{1/3}Nb_{2/3})O_3$) to metrically tetragonal $Sr_3Cu_1Nb_2O_9$ ($\equiv Sr(Cu_{1/3}Nb_{2/3})O_3$). Powder XRD traces as well as EPMA analysis of a sample of nominal composition $Sr_{1.11}Cu_{0.22}Nb_{0.67}O_3$ (see Fig. 1) synthesized midway between these two compositions, however, invariably showed that the synthesized specimen was clearly two phase, with the majority phase again corresponding to the end member of the SS-II solid solution and the other phase to an $Sr_4Nb_2O_9$ related phase. EPMA analysis of this perovskite-related solid solution phase gave a composition of $Sr_{0.99(2)}Cu_{0.32(1)}Nb_{0.68(2)}O_3$, again very close to the nominal $SrCu_{0.33}Nb_{0.67}O_3$ composition. The average of 10 separate analyses of the $Sr_4Nb_2O_9$-related phase gave a composition of $Sr_{1.21(6)}Cu_{0.06(2)}Nb_{0.69(4)}O_3$. A further single phase (to XRD) specimen within this $Sr_4Nb_2O_9$-related SS-III solid solution phase, of composition $Sr_{1.25(2)}Cu_{0.05(1)}Nb_{0.68(1)}O_3$ was also synthesized.

3.2. Powder XRD results

The compositions of typical single phase compounds representative of the SS-I, SS-II and SS-III solid solutions are $Sr_{0.99(2)}Cu_{0.41(1)}Nb_{0.60(1)}O_{2.90}$, $Sr_{0.98(2)}Cu_{0.34(2)}Nb_{0.67(1)}O_3$ and $Sr_{1.25(2)}Cu_{0.05(1)}Nb_{0.68(1)}O_3$. Line scans through experimental Guinier XRD patterns for each of these three single phase compounds are shown in Fig. 2 (keep in mind that the FWHM of the peaks in Fig. 2 have been broadened by the scanning process). In general, the weak additional satellite reflections observed in electron diffraction (see Section 3.3 below) are not apparent except in more heavily overexposed Guinier patterns. Indexation in Fig. 2 is thus with respect to the underlying (metrically distorted) perovskite parent sub-structure (subscript p).

$Sr_{0.99(2)}Cu_{0.41(1)}Nb_{0.60(1)}O_{2.90}$ was determined by Guinier powder XRD to be metrically cubic with $a = 3.9790(3)$ Å while the Cu-rich end-member of this narrow SS-I solid solution, of EPMA-determined composition $Sr_{0.98(3)}Cu_{0.42(2)}Nb_{0.59(2)}O_{2.88}$, was again determined to be metrically cubic with $a = 3.9756(3)$ Å. (No additional satellite reflections were detected in the Guinier patterns. Weak additional satellite reflections necessitating a doubling of these cell dimensions to 7.9580 and 7.9512 Å, respectively were, however, detected via electron diffraction—see Section 3.3 below.) Note that Sun et al. [8] reported

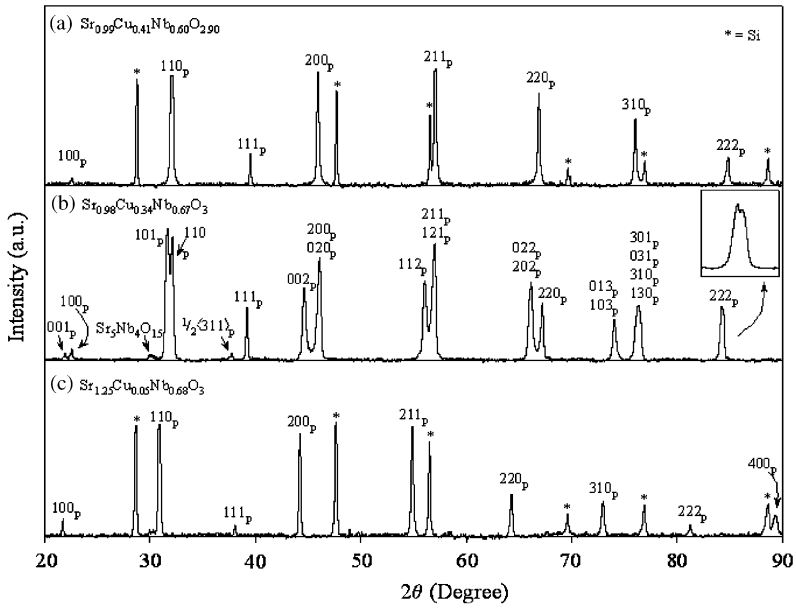

Fig. 2. Shows line scans through experimental Guinier XRD patterns for each of the three single phase compounds. In general, the weak additional satellite reflections observed in electron diffraction (see Section 3.3) are not apparent. Indexation is thus with respect to the underlying perovskite parent sub-structure (subscript p).

$a = 3.9800(1)$ Å for their nominally $Sr_2CuNbO_{6-\delta}$ specimen. We would expect Sun et al.'s metrically cubic phase to correspond to the Cu-rich end-member of the narrow SS-I solid solution (see Fig. 1). The closeness of the cubic cell dimension found for $Sr_{0.98(3)}Cu_{0.42(2)}Nb_{0.59(2)}O_{2.88}$ with that reported by Sun et al. is consistent with such an interpretation.

Tao and Irvine [9], on the other hand, reported a metrically tetragonal (although close to metrically cubic) $P4/mmm$, $a = 3.9608(4)$ Å, $c = 3.9757(2)$ Å structure for single phase $SrCu_{0.4}Nb_{0.6}O_{2.9}$. (A splitting of this magnitude, $(c-a)/a = 0.0038$, while small, should nonetheless be clearly apparent in our experimental Guinier pattern, particularly at high angle. The $2\,2\,0_p$ parent line for example, given the above reported cell dimensions, would split into two separate lines at $g = 0.7128$ and $0.7141\,Å^{-1}$, respectively (separated by $\Delta(2\theta) \sim 0.141°$ or ~ 0.25 mm for the Cu$K\alpha$ radiation used). Likewise the $3\,1\,0_p$ parent line would break into three separate lines at $g = 0.7957$, 0.7981 and $0.7984\,Å^{-1}$, respectively. The splitting of the former line from the latter two corresponds to $\Delta(2\theta) \sim 0.284°$ or ~ 0.5 mm for Cu$K\alpha$ radiation. Splittings of such magnitude would be readily detectable. No such splittings, however, were observed.)

Although their XRD data suggested a cubic $Pm3m$ structure, the symmetry was lowered to tetragonal as a result of "…visible extra broadening on peaks that would be expected to split under tetragonal distortion…" [9]. We did not find any such splitting or noticeable broadening in our Guinier XRD patterns. In order to investigate this conclusion more quantitatively, XRD data of the $Sr_{0.99(2)}Cu_{0.41(1)}Nb_{0.60(1)}O_{2.90}$ sample (as well as an included Si standard) was also carefully collected using a SIEMENS D-5000 diffractometer operating in Bragg–Brentano mode, a step size of 0.02° 2θ and a counting time of 5 s. The Cu$K\alpha_2$ contribution was subtracted electronically. The FWHM of the various observed reflections of the $Sr_{0.99(2)}Cu_{0.41(1)}Nb_{0.60(1)}O_{2.90}$ sample (open circles) as well as those of the included Si standard (triangles) were then measured and plotted as a function of 2θ as shown in Fig. 3. The open diamonds correspond to the

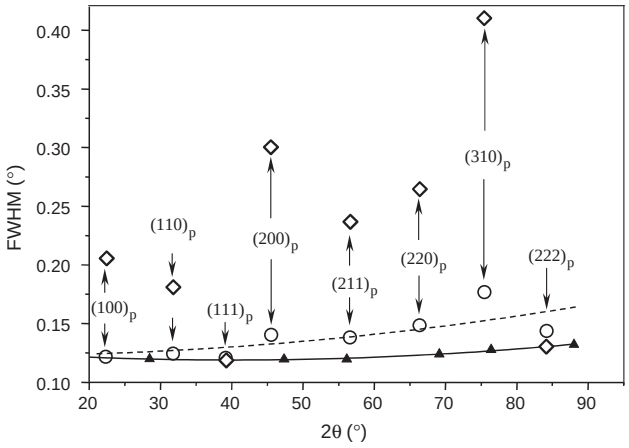

Fig. 3. Shows the measured FWHM of the various observed reflections for the $Sr_{0.99}Cu_{0.41}Nb_{0.60}O_{2.90}$ sample (open circles) as well as those of the included Si standard (triangles) plotted as a function of 2θ. The open diamonds correspond to the minimum FWHM that should be observed were the metrically tetragonal cell reported in Ref. [9] correct.

minimum FWHM that should be observed were the metrically tetragonal cell reported in Ref. [9] correct.

The Guinier powder pattern of the '$Sr_{0.98(2)}Cu_{0.34(2)}Nb_{0.67(1)}O_3$' compound (see Fig. 2) initially appeared relatively uncomplicated with no visible evidence for additional unexpected splitting of any of the parent perovskite lines or for the presence of any weak additional superstructure or impurity peaks. All of the lines could be indexed to a metrically tetragonal unit cell with $a_p = b_p = 3.9612(10)$ Å and $c_p = 4.0822(15)$ Å (see Fig. 2b), in good agreement with the earlier tetragonal cell dimensions reported for this composition by Venevtsev [7] and Fesenko et al. [10]. Some of the lines, however, were noticeably broadened (as reflected in the standard deviations just quoted; see also Fig. 2b) suggesting that the true local metric symmetry may be even lower than tetragonal. Annealing for longer periods of time than 24 h at 1300°C resulted in the emergence of a very small but quite reproducible splitting of the parent perovskite $\langle 222 \rangle_p^*$ reflection at high 2θ (indicative of a lowering of the metric symmetry of the parent perovskite sub-lattice from tetragonal to monoclinic or lower). Furthermore, a trace amount of an $Sr_5Nb_4O_{15}$ related phase (giving rise to a very weak impurity peak at $2\theta \sim 30°$ as previously reported by Tao and Irvine [9]) was detected in more heavily exposed Guinier films (see the reflection labelled '$Sr_5Nb_4O_{15}$' in Fig. 2b) as well as a weak superstructure reflection (labelled $\frac{1}{2}[311]_p^*$ in Fig. 2b). The presence of this latter superstructure reflection suggested a doubling of the above reported metrically tetragonal cell dimensions to a cell very close to $a = b = 7.9224$ Å and $c = 8.1644$ Å, respectively. It was not, however, possible to unambiguously assign a cell without the electron diffraction data reported in Section 3.3 below.

The single phase $Sr_{1.25}Cu_{0.05}Nb_{0.68}O_3$ sample was again metrically cubic (see Fig. 2c). The presence of weak additional lines in EDPs (see Section 3.3 below) and heavily exposed Guinier patterns, however, necessitated a doubling of the parent perovskite cell dimension to $a = 8.2403(14)$ Å. This is in good agreement with the recently reported, metrically cubic ($a = 8.2682(2)$ Å) high-temperature phase of $Sr_4Nb_2O_9$ [13].

3.3. Electron diffraction results

Fig. 4 shows typical (a) $\langle 001 \rangle$, (b) close to $\langle 001 \rangle$, (c) $\langle 0\bar{1}3 \rangle$ and (d) $\langle 0\bar{1}\bar{1} \rangle$ zone axis EDPs of $Sr_{0.99(2)}Cu_{0.41(1)}Nb_{0.60(1)}O_{2.90}$ and of the SS-I solid solution. Indexation with the subscript p in Fig. 4 is

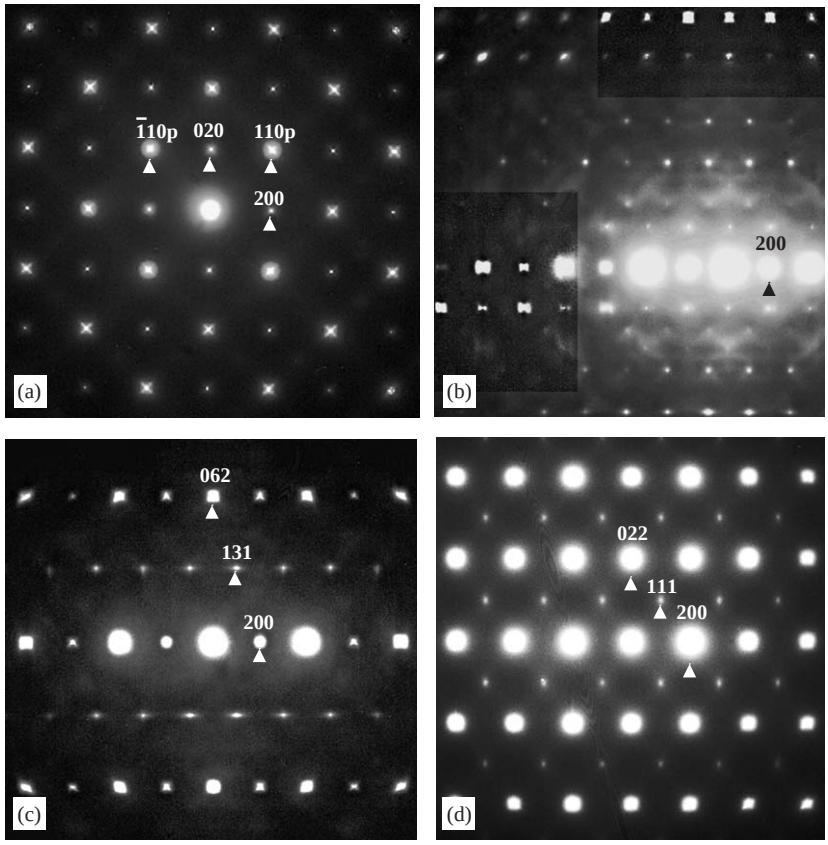

Fig. 4. (a) $\langle 001 \rangle$, (b) close to $\langle 001 \rangle$, (c) $\langle 0\bar{1}3 \rangle$ and (d) $\langle 0\bar{1}1 \rangle$ zone EDPs typical of $Sr_{0.99}Cu_{0.41}Nb_{0.60}O_{2.90}$ and of the SS-I solid solution. Indexation with the subscript p is with respect to the underlying perovskite type parent structure while that without the subscript p is with respect to an $a = 2a_p$ supercell.

with respect to the underlying metrically cubic, perovskite type parent structure. Note the very weak but quite reproducible presence of $\mathbf{G} \pm 1/2\langle 111\rangle_p^*$ ($\mathbf{G}$ a parent perovskite Bragg reflection) satellite reflections in (c) and (d) necessitating a doubling of the cubic cell dimension to $a = 2a_p$ ($=7.9580\,\text{Å}$ for $Sr_{0.99(2)}Cu_{0.41(1)}Nb_{0.60(1)}O_{2.90}$ and $7.9512\,\text{Å}$ for $Sr_{0.98(3)}Cu_{0.42(2)}Nb_{0.59(2)}O_{2.88}$). Indexation without the subscript p in Fig. 4 is with respect to this latter cell. The only systematic extinction condition observed requires an *F*-centered Bravais lattice. No evidence could be found to justify lowering of the Laue symmetry from *m*3*m* i.e. all $\langle 001\rangle_p$, $\langle 110\rangle_p$, etc. *m*3*m* symmetry related orientations gave equivalent EDPs in both selected area and microdiffraction mode. In conjunction with the cubic metric symmetry, the most likely space group symmetry is thus *Fm*3*m*. Such a space group symmetry is well-known for $A_2BB'O_6$ double perovskites [14] and is compatible with a tendency for Cu and Nb to alternate along each of the three $\langle 001\rangle$ directions. Given the non-1:1 *B*-site stoichiometry, however, such ordering cannot be perfect.

Note the presence of weak but quite reproducible diffuse streaking (of quite short length) running through the Bragg reflections perpendicular to the $\langle 110\rangle^*$ directions of reciprocal space (particularly apparent in (a) and (c)). Such diffuse scattering is strongly reminiscent of materials on the threshold of a ferroelastic phase transition from a high symmetry to a lower symmetry structure [15,16] and is usually associated in real space with the existence of a tweed microstructure, the precursor to a long range ordered lowering of symmetry. It is also absolutely characteristic of this SS-I phase.

Finally note the appearance of "*bow–tie* like" diffraction features in the close to $\langle 001\rangle$ zone axis EDP of Fig. 4b. Such diffraction features are reminiscent of similar diffraction features arising from so-called 'atomic size effect' structural relaxations that occur in yttria-stabilized cubic zirconia [17,18]. The azimuthal intensity variation of the "*bow–tie* like" diffraction features suggests that they are associated with local contraction/dilation of the average structure lattice [17,18], presumably a result of local Cu/Nb ordering on the *B* sites. The disappearance of the "*bow–tie* like" diffraction features at the exact $\langle 001\rangle$ zone axis orientation requires that there is no such local contraction/dilation of the average structure lattice in projection.

Fig. 5 shows (a) [001], (b) $[\bar{1}10]$, (c) [201] and (d) [100] zone axis EDPs of $Sr_{0.98(2)}Cu_{0.34(2)}Nb_{0.67(1)}O_3$ and characteristic of the narrow SS-II solid solution. Indexation with the subscript p in Fig. 5 is again with

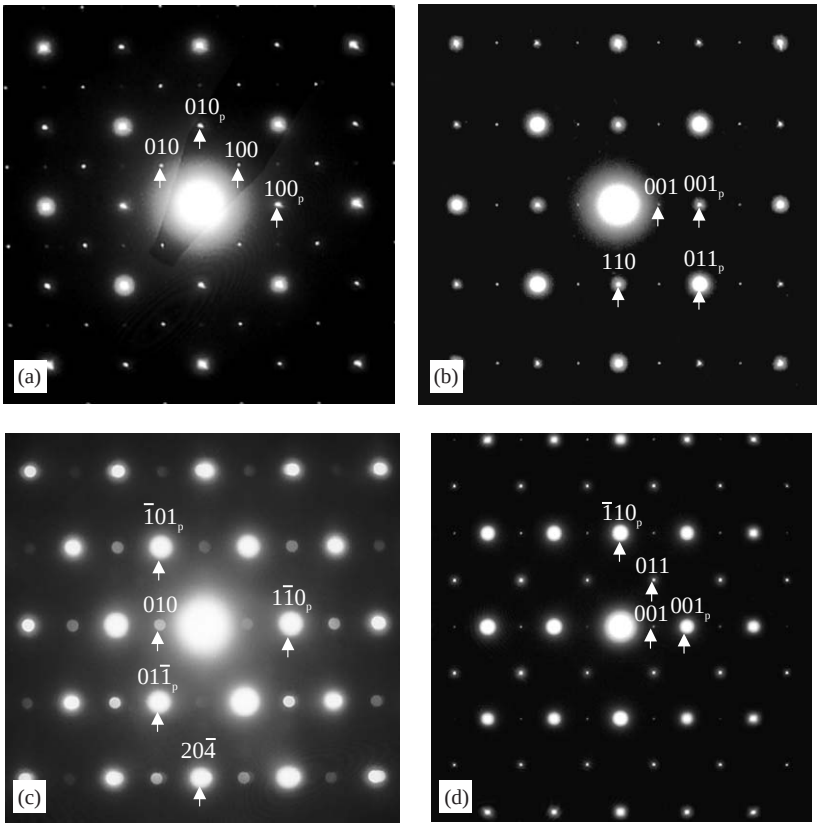

Fig. 5. EDPs of $Sr_{0.98}Cu_{0.34}Nb_{0.67}O_3$ and typical of the narrow SS-II solid solution: (a) [001], (b) $[\bar{1}10]$, (c) [201] and (d) [100]. Indexation with the subscript p is with respect to the underlying perovskite type parent structure. Indexation without the subscript p is with respect to a $\sqrt{2}a_p \times \sqrt{2}a_p \times 2a_p$ ($\mathbf{a} = \mathbf{a}_p + \mathbf{b}_p$, $\mathbf{b} = -\mathbf{a}_p + \mathbf{b}_p$, $\mathbf{c} = 2\mathbf{c}_p$; $\mathbf{a}^* = 1/2[110]_p^*$, $\mathbf{b}^* = \frac{1}{2}[\bar{1}10]_p^*$, $\mathbf{c}^* = 1/2[001]_p^*$) supercell.

respect to the underlying perovskite type parent structure. Indexation without the subscript p is with respect to a *P*-centered, $\sqrt{2}a_p \times \sqrt{2}a_p \times 2a_p$ ($\mathbf{a} = \mathbf{a}_p + \mathbf{b}_p$, $\mathbf{b} = -\mathbf{a}_p + \mathbf{b}_p$, $\mathbf{c} = 2\mathbf{c}_p$; $\mathbf{a}^* = \frac{1}{2}[110]^*_p$, $\mathbf{b}^* = \frac{1}{2}[\bar{1}10]^*_p$, $\mathbf{c}^* = \frac{1}{2}[001]^*_p$) supercell. Tao and Irvine [9] also reported that the main phase at this composition was a "…tetragonal perovskite with lattice parameters $\sqrt{2}a_p \times \sqrt{2}a_p \times 2a_p$…" although no space group or cell dimensions were given. Such a supercell is at first sight surprising given the 1:2 B site stoichiometry. A $\sqrt{2}a_p \times \sqrt{2}a_p \times 2a_p$ supercell is much more commonly associated with 1:1 *B*-site ordered, perovskite-related superstructure phases of space group symmetry $P12_1/n1$ with $\mathbf{a} = \mathbf{a}_p + \mathbf{b}_p$, $\mathbf{b} = -\mathbf{a}_p + \mathbf{b}_p$ and $\mathbf{c} = 2\mathbf{c}_p$ (see, e.g., Ref. [14] and references contained therein).

Given the $\sqrt{2}a_p \times \sqrt{2}a_p \times 2a_p$ supercell and the very close to tetragonal metric symmetry ($a_p = 3.9612(10)$ Å and $c_p = 4.0822(15)$ Å) found by powder XRD (see Fig. 2), it was expected that the metrically unique $\langle 001 \rangle_p$ axis would correspond to $[001]_p$. Careful, and repeated, measurement of $\langle 001 \rangle_p$ type zone axis EDPs such as those shown in Figs. 5a and b, however, shows that this metrically unique axis in fact corresponds to the $[100]_p$ direction in the setting we have used, i.e., $a^*_p < b^*_p = c^*_p$. A metrically tetragonal ($b_p = c_p = 3.9612(10)$ Å, $a_p = 4.0822(15)$ Å) parent unit cell implies, e.g., that $\mathbf{a}^*_p \cdot \mathbf{b}^*_p \equiv (\mathbf{a}^* - \mathbf{b}^*) \cdot (\mathbf{a}^* + \mathbf{b}^*) = 0$, i.e., $a^* = b^*$ while a^*_p ($= 1/4.0822$ Å) $< b^*_p = c^*_p$ ($= 1/3.9612$ Å) requires that $a^* = b^* = 0.1759$ Å^{-1}, $c^* = 0.1262$ Å^{-1}, $\alpha^* = \beta^* = 90°$ and $\gamma^* \neq 90° \sim 88.28°$ (i.e., $a = b = 5.6882$, $c = 7.9224$ Å, $\alpha = \beta = 90°$ and $\gamma \sim 91.7237°$ for $Sr_{0.98(2)}Cu_{0.34(2)}Nb_{0.67(1)}O_3$). That $\gamma^* \neq 90° \sim 88.28°$ can be measured directly from Fig. 5a but is even more apparent from the four-fold twinned [001] zone axis EDP shown in Fig. 6. With respect to this $\sqrt{2}a_p \times \sqrt{2}a_p \times 2a_p$ ($\mathbf{a} = \mathbf{a}_p + \mathbf{b}_p$, $\mathbf{b} = -\mathbf{a}_p + \mathbf{b}_p$, $\mathbf{c} = 2\mathbf{c}_p$) supercell, the true resultant space group symmetry of this phase is thus at most monoclinic $P11m$ or $P112/m$ (with the unique monoclinic axis as **c**) despite the apparent tetragonal metric symmetry of the parent sub-structure.

Alternatively, one could define a new C-centered ($\mathbf{a}' = 2\mathbf{a}_p$, $\mathbf{b}' = 2\mathbf{b}_p$, $\mathbf{c}' = 2\mathbf{c}_p$; $a' = 8.1644$, $b' = 7.9224$ Å, $c' = 7.9224$ Å, $\alpha' = \beta' = \gamma' = 90°$ for $Sr_{0.99(3)}Cu_{0.41(2)}Nb_{0.60(2)}O_{2.90}$) orthorhombic supercell (of space group symmetry *Cmmm* or a C-centered sub-group thereof) that would also be compatible with the observed EDPs as well as the apparent tetragonal metric symmetry (see Fig. 2). The small but distinct splitting of the parent $\langle 222 \rangle^*_p$ reflection (see the inset to Fig. 2), however, requires that the true local symmetry is even lower still, i.e., C-centered monoclinic or lower. Higher resolution synchrotron XRD data, beyond the scope of the current paper, is needed to go further.

Fig. 7 shows (a) $\langle 1\bar{1}0 \rangle$, (b) close to $\langle 001 \rangle$, (c) $\langle \bar{1}\bar{1}2 \rangle$, (d) $\langle \bar{3}31 \rangle$, (e) $\langle 13\bar{2} \rangle$ and (f) $\langle \bar{2}30 \rangle$ zone axis EDPs of $Sr_{1.28}Cu_{0.05}Nb_{0.67}O_3$ but typical of the SS-III solid solution. As for SS-I, the weak but quite reproducible presence of $\mathbf{G} \pm 1/2\langle 1\,1\,1 \rangle^*_p$ (**G** a parent perovskite Bragg reflection) satellite reflections necessitated a doubling of the cubic cell dimension to $a = 2a_p$ ($= 8.2403$ Å for $Sr_{1.28}Cu_{0.05}Nb_{0.67}O_3$). Indexation in Fig. 7 is with respect to this doubled cell. The only observed systematic extinction conditions require an *F*-centered Bravais lattice. As for SS-I, no evidence was found for lowering of the Laue symmetry from *m*3*m*, i.e. all $\langle 001 \rangle$, $\langle 110 \rangle$, etc. *m*3*m* symmetry related orientations gave equivalent EDPs. In conjunction with the cubic metric symmetry, the most likely space group symmetry is thus *Fm*3*m*. This is in agreement with the recently reported *Fm*3*m*, $a = 2a_p$, average crystal structure of the high-temperature polymorph of $Sr_{1.33}Nb_{0.67}O_3$ ($Sr_4Nb_2O_9$) [13].

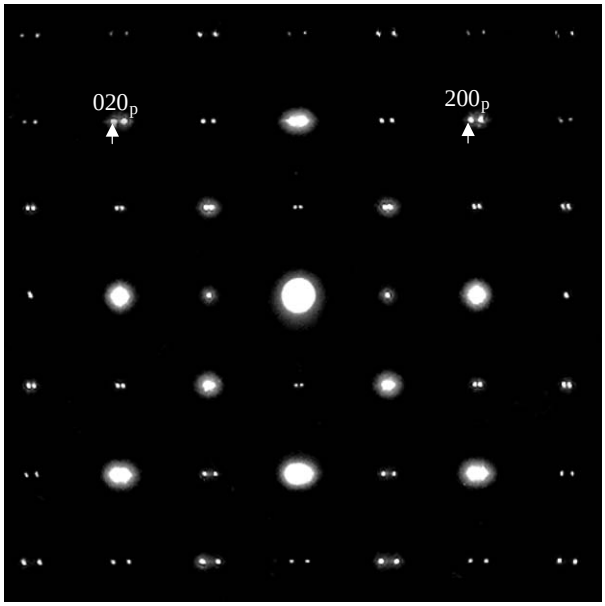

Fig. 6. Four-fold twinned [001] zone axis EDP of $Sr_{0.98}Cu_{0.34}Nb_{0.67}O_3$. The observed splitting confirms that the angle between $[100]^*$ and $[010]^*$ in Fig. 3a cannot be 90°.

Also in agreement with this latter study is the presence of a spectacular, highly structured, characteristic diffuse intensity distribution indicative of extensive local short range order and associated structural relaxation [19,20]. As pointed out by Levin et al. [13], the observed diffuse intensity appears to concentrate on a surface closely related to the so-called *P* minimal surface in reciprocal space (see Fig. 5 of [13] or Fig. 1 of [19]). While this is certainly true for some zone axis orientations (cf., for example, Fig. 7d with Fig. 4a of [20] or Fig. 7e with Fig. 3f of [19]), there are nonetheless also significant differences (cf., for example, Fig. 7a with Fig. 3b of [19] or Fig. 4a of [20], Fig. 7b with Fig. 3a of [19] or Fig. 7c with Fig. 3h of [19]). Clearly much still remains to be understood about the nature of the short range ordering and associated structural relaxation responsible for this spectacular diffuse intensity distribution.

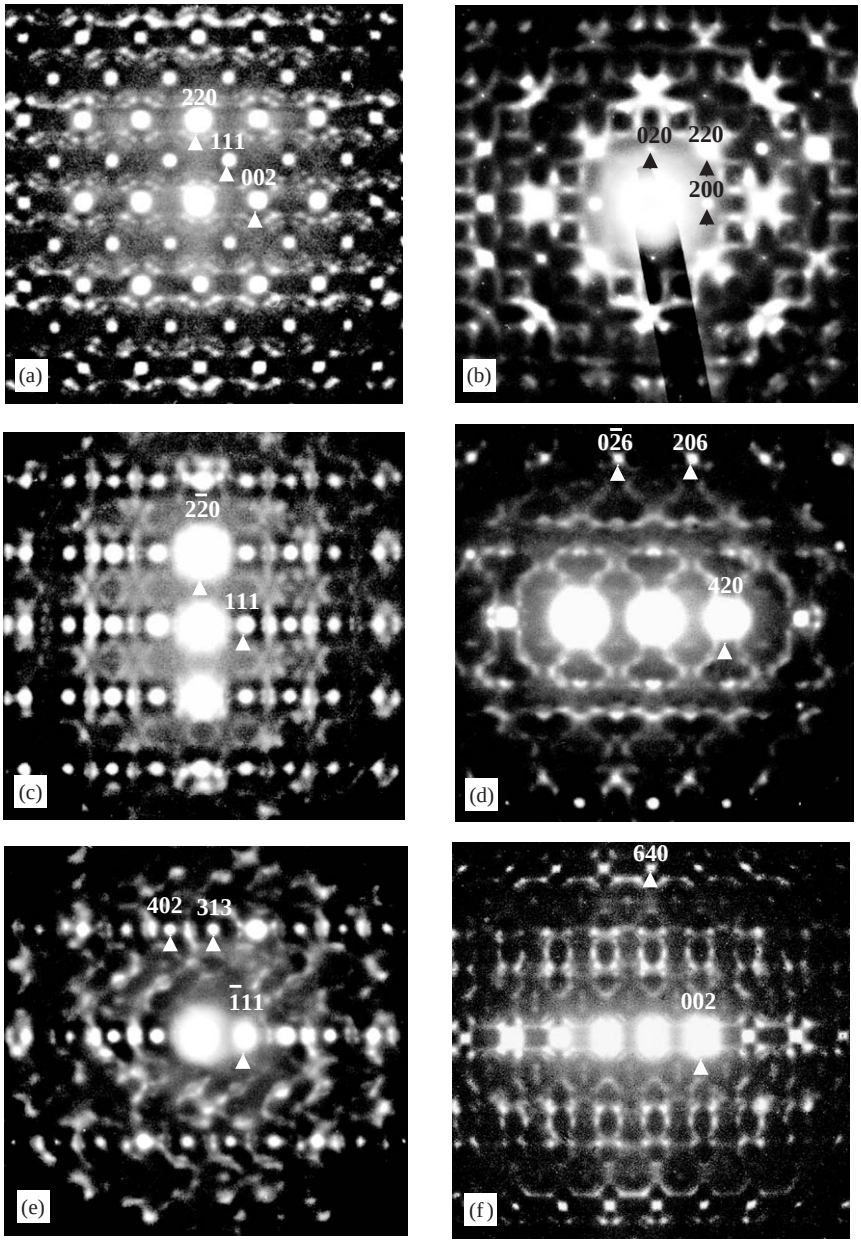

Fig. 7. EDPs of $Sr_{1.25}Cu_{0.05}Nb_{0.68}O_3$ but typical of the SS-III solid solution: (a) $\langle 1\bar{1}0 \rangle$, (b) close to $\langle 001 \rangle$, (c) $\langle \bar{1}\bar{1}2 \rangle$, (d) $\langle \bar{3}31 \rangle$, (e) $\langle 13\bar{2} \rangle$ and (f) $\langle \bar{2}30 \rangle$ zone axis. Indexation is with respect to a doubled $a = 2a_p$ cell.

In summary then, the SS-I solid solution is characterized by an *F*-centered, $a = 2a_p$ (= 7.9580 Å for $Sr_{0.99(2)}Cu_{0.41(1)}Nb_{0.60(1)}O_{2.90}$ and 7.9512 Å for $Sr_{0.98(3)}Cu_{0.42(2)}Nb_{0.59(2)}O_{2.88}$) cell. The most likely space group symmetry is *Fm*3*m*. The SS-II solid solution is characterized by a *P*-centered, $\mathbf{a} = \mathbf{a}_p + \mathbf{b}_p$, $\mathbf{b} = -\mathbf{a}_p + \mathbf{b}_p$, $\mathbf{c} = 2\mathbf{c}_p$ ($a = b = 5.6882$, $c = 7.9224$ Å, $\alpha = \beta = 90°$ and $\gamma \sim 91.7237°$ for $Sr_{0.98(2)}Cu_{0.34(2)}Nb_{0.67(1)}O_3$) supercell. The highest possible space group symmetry is $P112/m$ (with the unique monoclinic axis as **c**). The SS-III solid solution is characterized by an *F*-centered $a = 2a_p$ (= 8.2403 Å for $Sr_{1.28}Cu_{0.05}Nb_{0.67}O_3$) supercell. As for SS-I, the most likely space group symmetry is *Fm*3*m*.

The quite distinct electron diffraction characteristics of each of the three cubic perovskite-related solid solutions described above confirm the EPMA and phase analysis results described in Section 3.1 above, i.e. there exist three quite distinct cubic perovskite-related solid solution phases in the SrO–CuO–Nb_2O_5 sytem.

3.4. Conductivity results

Finally, Arrhenius plots of electrical conductivity versus $1/T$ are presented for $Sr_{0.99(2)}Cu_{0.41(1)}Nb_{0.60(1)}O_{2.90}$ (SS-I), $Sr_{0.98(2)}Cu_{0.34(2)}Nb_{0.67(1)}O_3$ (SS-II) and $Sr_{1.25(2)}Cu_{0.05(1)}Nb_{0.68(1)}O_3$ (SS-III) in Fig. 8. The

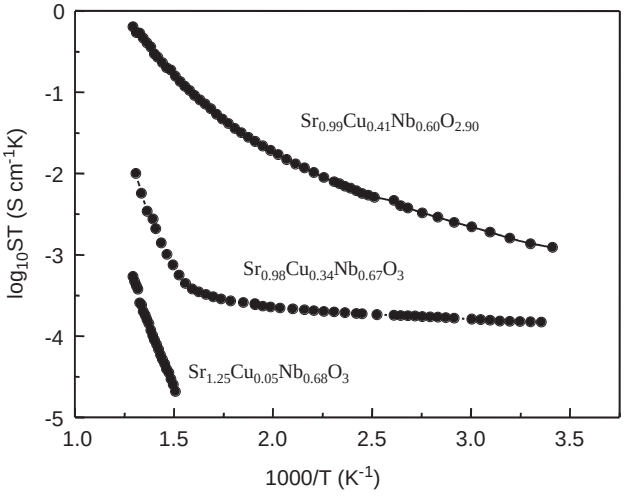

Fig. 8. Arrhenius plots of electrical conductivity versus $1/T$ for $Sr_{0.99}Cu_{0.41}Nb_{0.60}O_{2.90}$, $Sr_{0.98(2)}Cu_{0.34(2)}Nb_{0.67(1)}O_3$ and $Sr_{1.25}Cu_{0.05}Nb_{0.68}O_3$.

electrical conductivity of $Sr_{0.99(2)}Cu_{0.41(1)}Nb_{0.60(1)}O_{2.90}$ is $4\times10^{-6}\,S\,cm^{-1}$ at room temperature and increases with increasing temperature, consistent with semi-conducting behavior. Thermal voltage measurements indicate that $Sr_{0.99(2)}Cu_{0.41(1)}Nb_{0.60(1)}O_{2.90}$ is an n-type semiconductor, in agreement with Tao and Irvine [9]. $Sr_{0.98(2)}Cu_{0.34(2)}Nb_{0.67(1)}O_3$, by contrast, shows a very low electrical conductivity of $5.3\times10^{-7}\,S\,cm^{-1}$ at room temperature which does not increase over most of the measured temperature range up until $\sim650^{\circ}K$. Thus, despite the small variation in composition between the SS-I and SS-II solid solutions, they display quite distinct electrical properties. In the case of $Sr_{1.25(2)}Cu_{0.05(1)}Nb_{0.68(1)}O_3$, the resistance exceeded the $30\,M\Omega$ maximum measurable on our apparatus over most of the measured temperature range, i.e. up until $\sim660^{\circ}K$. Again the three perovskite-related solid solutions display quite distinct electrical characteristics.

4. Conclusion

Three quite distinct cubic perovskite-related solid solutions have been found in the $SrO–CuO–Nb_2O_5$ system, each with quite distinct electrical and structural characteristics.

References

[1] J.G. Bednorz, K.A. Muller, Z. Phys. B 64 (1986) 189.
[2] H. Muller-Buschbaum, Angew. Chem. Int. Ed. Engl. 30 (1991) 723.
[3] M.-H. Julien, Physica B: Condens. Matter 329–333 (2003) 693.
[4] Y. Tokura, Physica C: Supercond. 185–189 (1991) 174.
[5] A.G. Loeser, Z.-X. Shen, D.S. Dessau, W.E. Spicer, J. Electron Spectrosc. Relat. Phenom. 66 (1994) 359.
[6] H. Rietschel, J. Fink, E. Gering, F. Gompf, N. Nocker, L. Pintschovius, B. Renker, W. Reichardt, H. Schmidt, W. Weber, Physica C: Supercond. 153–155 (1988) 1067.
[7] Y.N. Venevtsev, Mater. Res. Bull. 6 (1971) 1085.
[8] Z. Sun, X.H. Chen, R. Fan, X.G. Luo, L. Li, J. Phys. Chem. Solids 64 (2003) 59.
[9] S. Tao, J.T.S. Irvine, Solid State Ionics 154–155 (2002) 659.
[10] E.G. Fesenko, V.G. Smotrakov, V.V. Eremkin, L.A. Shilkina, Inorg. Mater. 28 (1992) 1751.
[11] A.L. Podkorytov, M.I. Pantyukhina, V.M. Zhukovskii, V.V. Simonov, Russ. J. Inorg. Chem. 39 (1994) 1492.
[12] B. Noläng, Inst. Materialkemi, Ängströmlaboratoriet, Box 538, SE-751 21, Uppsala, Sweden.
[13] I. Levin, J.Y. Chan, J.H. Scott, L. Farber, T.A. Vanderah, J.E. Maslar, J. Solid State Chem. 166 (2002) 24.
[14] M.T. Anderson, K.B. Grenwood, G.A. Taylor, K.R. Poeppelmeier, Prog. Solid State Chem. 160 (1993) 197.
[15] R.L. Withers, S. Schmid, J.G. Thompson, in: J.N. Boland, J.D. Fitz Gerald (Eds.), Defects and Processes in the Solid State: Geoscience Applications: The McLaren Volume, Elsevier, Amsterdam, 1993, p. 305.
[16] J. Zhang, L. Liu, C. Dong, J. Li, H. Chen, X. Li, G. Cheng, Phys. Rev. B 65 (2002) 054513-1.
[17] T.R. Welberry, R.L. Withers, J.G. Thompson, B.D. Butler, J. Solid State Chem. 100 (1992) 71.
[18] T.R. Welberry, B.D. Butler, J.G. Thompson, R.L. Withers, J. Solid State Chem. 106 (1993) 461.
[19] M. Sauvage, E. Parthé, Acta Crystallogr. A 28 (1972) 607.
[20] R.L. Withers, T.R. Welberry, F.J. Brink, L. Norén, J. Solid State Chem. 170 (2003) 211.